CHEMISTRY OF MATERIALS
ARTICLE
pubs.acs.org/cm

Functionalization of Multiwalled Carbon Nanotubes with Cyclic Nitrones for Materials and Composites: Addressing the Role of CNT Sidewall Defects

Giuliano Giambastiani,[*,†] Stefano Cicchi,[*,‡] Alessandra Giannasi,[§] Lapo Luconi,[†] Andrea Rossin,[†] Francesco Mercuri,[⊥] Claudio Bianchini,[†] Alberto Brandi,[‡] Manuela Melucci,[†] Giacomo Ghini,[†] Paola Stagnaro,[‖] Lucia Conzatti,[‖] Elisa Passaglia,[○] Marco Zoppi,[§] Tiziano Montini,[▽] and Paolo Fornasiero[▽]

[†]Istituto di Chimica dei Composti Organometallici (ICCOM-CNR), Via Madonna del Piano 10, 50019 — Sesto Fiorentino (Firenze), Italy

[‡]Dipartimento di Chimica "U. Schiff", Università degli Studi di Firenze, Via della Lastruccia, 13, 50019 — Sesto Fiorentino (Firenze), Italy

[§]Istituto dei Sistemi Complessi (ISC—CNR), Via Madonna del Piano 10, 50019 — Sesto Fiorentino (Firenze), Italy

[⊥]Istituto di Scienze e Tecnologie Molecolari (ISTM-CNR) and UdR INSTM, c/o Dipartimento di Chimica, Università degli Studi di Perugia, Via Elce di Sotto 8, 06123 — (Perugia), Italy

[‖]Istituto per lo Studio delle Macromolecole (ISMAC—CNR), UOS Genova — Via De Marini 6, 16149 — (Genova), Italy

[○]Istituto di Chimica dei Composti Organometallici (ICCOM-CNR), UOS Pisa — Via Moruzzi 1 and Università degli Studi di Pisa, Via Risorgimento 35, 56126 — (Pisa), Italy

[▽]Istituto di Chimica dei Composti Organometallici (ICCOM-CNR), UOS Trieste, c/o Dipartimento di Scienze Chimiche e Farmaceutiche, Università di Trieste, Via L. Giorgieri 1, 34127 — (Trieste), Italy

Supporting Information

ABSTRACT: An efficient approach to the organic functionalization of multiwalled carbon nanotubes (MWCNTs) for the production of highly soluble/dispersible materials has been accomplished by a class of highly reactive and thermally stable nitrones. Besides the unprecedented solubility in aprotic polar solvents of the functionalized samples (up to 10 mg of *f*-MWCNTs per mL of DMF), we have demonstrated, for the first time, that the CNT functionalization by nitrones preferentially occurs at the defective CNT sidewalls without any appreciable degradation of their sp^2 network. The role of the reticular imperfections on the graphitic lattice of the MWCNTs has been experimentally and theoretically addressed. A complete chemical (TGA-MS, FT-IR, SSA) and morphological (TEM, AFM) characterization of the functionalized materials has accounted for the high degree of CNT functionalization, whereas Raman scattering, in combination with complementary XRPD and active surface area (ASA) measurements, has provided unambiguous evidence of the key role played by the structural "disorder" of the MWCNTs in the nitrone cycloaddition. Density functional theory (DFT) calculations on the reactivity of selected topological defects at the CNT sidewalls have contributed to trace-out a "defect-based" sidewall reactivity trend. The excellent processability of the functionalized MWCNTs has been finally exploited for the preparation of highly homogeneous CNT/polymer nanocomposites with CNT loadings as high as 3 wt %.

KEYWORDS: MWCNTs, nitrones, 1,3-dipolar cycloaddition, topological defects, Raman, ASA, DFT calculations

■ INTRODUCTION

Since their discovery,[1] carbon nanotubes (CNTs)[2] have received growing attention in nanotechnology, because of their unique mechanical, thermal, and electrical properties.[3,4] Currently, CNTs are among the nanomaterials with the largest impact on a wide range of technological applications. In particular, their incorporation, even in small amounts, into other (macromolecular) materials has been found to improve the thermal stability[5−7] and mechanical properties[8−10] of the resulting composites. The major drawback in the use of pristine CNTs is related to their scarce processability and miscibility in the most common media. Relevant intersupramolecular interactions between the tubes are actually responsible for self-aggregation effects, which ultimately prevent their homogeneous dispersion in solution or in host polymeric matrices.

Received: December 23, 2010
Published: March 02, 2011

The chemical functionalization of the CNT sidewalls is a well-established approach to facilitate the material manipulation and improve both its dispersibility in organic solvents/water and processability with other macromolecular materials. The chemical functionalization allows for a tuning of the CNTs chemical and physical properties, and also represents an efficient method for their purification. The development of new methodologies for the covalent functionalization of CNTs, aimed at integrating these nanomaterials into more-complex functional structures, has recently emerged as an area of great interest.[11] In this respect, much attention is being paid to the covalent attachment of organic fragments to the π-conjugated skeleton of single-walled carbon nanotubes (SWCNTs) and multiwalled carbon nanotubes (MWCNTs).[12] Nevertheless, the latter, which are more suitable for specific technological applications such as the production of polymer-based nanocomposites, are less investigated, because of their typically higher curvature radius and related macromolecular architecture complexity. These features are responsible for reduced sidewall chemical reactivity and a more difficult characterization of the resulting functionalized materials.

Despite the high chemical inertness of the CNT sidewalls, some relevant examples of organic functionalization have been successfully addressed.[11] The methods exploited so far include the treatment with nitrenes,[13] nucleophilic carbenes,[14] diazonium salts,[15] bromomalonates,[16] and free radicals.[17] In particular, 1,3-dipolar cycloadditions[18] represent a special class of organic reactions whose applicability to the CNT functionalization is well-documented in several theoretical[19,20] and experimental[21−24] reports. The cycloaddition of azomethine ylides onto SWCNTs or MWCNTs represents a powerful tool for producing highly soluble and pure CNTs.[22,23] Calculated reaction energies and barriers for the cycloaddition of other 1,3-dipoles to a model armchair (5,5) SWCNT predict that ozone, nitrile ylide, and nitrile imine are also good candidates for the CNT functionalization.[19] In contrast, unfavorable energy balances (high activation energy and relatively low energy barrier for the retro-cycloaddition process) make nitrone cycloaddition less feasible, compared to other dipoles.[19] Although it is generally accepted that the chemical reactivity of CNTs depends, in principle, on the CNT sidewall curvature,[25−28] the 1,3-dipole reactivity versus the CNT curvature still remains a subject to be unravelled. Our preliminary studies on the 1,3-dipolar cycloaddition of a highly reactive and thermally stable cyclic nitrone (namely, (3*S*,4*S*)-3,4-di-*tert*-butoxy-3,4-dihydro-2*H*-pyrrole *N*-oxide **1**[29]), to SWCNTs and MWCNTs have shown unexpected reactivity trends.[30] Attempts to functionalize SWCNTs using nitrone **1** were unsuccessful, while highly functionalized materials with unprecedented solubility/dispersibility in organic solvents have been prepared from the functionalization of MWCNTs. Notably, an in-depth characterization of the functionalized materials has suggested that the diffuse structural defects on the carbon sidewall lattice of the MWCNTs act as preferential reactive sites for the formation of the covalent bonds, preserving the crystal domain size of the sp^2 network.[30]

In the present work, we report a full account on the 1,3-dipolar cycloaddition to MWCNTs using two stereohomogeneous cyclic nitrones (**1** and **2**; see Scheme 1), the derivatization of the functionalized materials (*f*-MWCNTs) (Scheme 1), their detailed characterization and use for the production of polymer-based nanocomposites. Theoretical DFT calculations have been accomplished to shed light on the role of the “disordered carbon” at the MWCNT sidewall, with respect to its chemical reactivity in the nitrone cycloaddition reaction.

Scheme 1

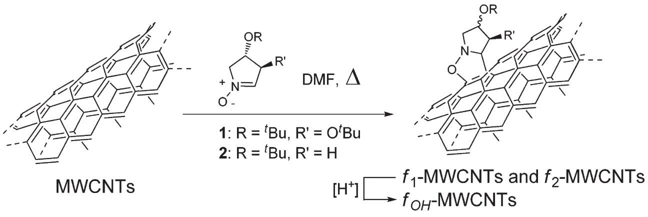

A morphological [atomic force microscopy (AFM), transmission electron microscopy (TEM), specific surface area (SSA)] and chemico-physical (Raman spectroscopy, X-ray powder diffraction (XRPD), active surface area (ASA)) surface characterization of the MWCNTs, before and after functionalization, has been carried out to obtain information on the relationships between the surface structure and the chemical reactivity of these macromolecular systems. All the collected data led us to conclude that much of the chemical reactivity preferentially occurs at the CNT surface defect sites.

Finally, the extremely high solubility/dispersibility of selected nitrone-functionalized MWCNTs has been applied to the preparation of homogeneous polymer-based composites with a CNT loading up to 3 wt %. Morphological (TEM) and thermal [differential thermal analysis (DSC) and thermogravimetric analysis (TGA)] investigations on the resulting composites are presented and discussed.

EXPERIMENTAL SECTION

General Considerations. All manipulations were carried out under dry nitrogen atmosphere using standard Schlenk-type techniques. Nitrogen (≥99.999% from Rivoira) was dried through a $CaCl_2$ column and deoxygenated with an oxisorb cartridge from Messer Griesheim prior to use. Anhydrous toluene was obtained by means of an MBraun Solvent Purification System. Dry dimethylformamide (DMF) was prepared according to the literature procedure[31] and stored over 4 Å molecular sieves under a nitrogen atmosphere. MWCNTs (>90% carbon basis, provided by Sigma−Aldrich) were previously dried at 80 °C under reduced pressure (1.3×10^{-3} bar) for 8 h, then stored under N_2 atmosphere. Unless otherwise stated, all other chemicals were purchased from commercial suppliers and used as received without further purification. Nitrones **1** and **2** were prepared in a multigram scale, according to literature procedures.[29] Samples sonication was carried out using a Julabo USR3 Labortechnic bath sonicator (35 kHz, Power 2 × 150 W), cooling the samples in a water/ice mixture throughout the sample treatment. *Note: All measurements carried out on pristine MWCNTs and functionalized f-MWCNTs were conducted on samples that underwent identical washing/filtration/sonication/workup procedures.* Filtration was done through either a 100-nm-pore polycarbonate membrane (Millipore) or a 200-nm-pore Teflon membrane (Millipore).

Material Characterization and Analyses Conditions. TGA was performed under N_2 atmosphere (50 mL/min) on an EXSTAR Thermo Gravimetric Analyzer (TG/DTA) Seiko 6200 coupled with a ThermoStar GSD 301 T (TGA-MS) for mass spectroscopy (MS) gas analysis of volatiles. DSC measurements were carried out using a Perkin−Elmer DSC-7 differential scanning calorimeter. The samples were heated from 60 °C to 180 °C to eliminate their thermal history then cooled to 30 °C and heated again to 200 °C at a cooling/heating rate of

20 °C/min. Thermal scans were performed under nitrogen atmosphere after instrument calibration, carried out using indium (T_m = 156.60 °C) and zinc (T_m = 419.47 °C) as standards. TEM analysis of modified and unmodified CNTs was performed using a Philips CM12 microscope operating at 120 kV, on samples prepared by drop casting of previously sonicated suspensions over carbon-coated grids. TEM images were recorded with a CCD camera (Gatan 791). TEM analysis on CNT/PVPy composites was performed using a Zeiss EM 900 instrument by applying an accelerating voltage of 80 kV. Ultrathin sections (~50 nm thick) of film specimens embedded in an epoxy resin were prepared with a Leica EM FCS cryoultramicrotome that was equipped with a diamond knife. The sample was maintained at −60 °C, and the knife was maintained at −25 °C. AFM analysis was performed using a Park System XE-100E AFM instrument, on samples prepared by spin-coating (4200 rpm, 20 s) previously sonicated sample suspensions on freshly cleaved mica substrates. The AFM images were recorded with standard tips (Veeco Tips NCHV-A) in tapping mode at a scan rate of 1.0 Hz. Raman spectroscopy measurements were carried out using the green line (514.5 nm) of an Ar-ion laser. Spectra were obtained using a Spex Triplemate spectrometer that was equipped with high-resolution holographic gratings, and recorded using a liquid nitrogen-cooled CCD (Symphony Horiba Jobin Yvon). The overall spectral resolution was 1.3 cm^{-1}. All samples were maintained at constant room temperature (23 °C) and under helium atmosphere (3 bar) during the experiment;[32] an inert atmosphere was used to prevent undesired carbon oxidation, induced by possible local laser heating, which, in turn, was greatly reduced by the enhanced thermal conductivity of the pressurized gas. The Raman spectra were collected to detect the presence and strength of the G and D modes.[33] The G mode, which is located at ~1580 cm^{-1}, is characteristic of the sp^2 in-plane bond-stretching motion of pairs of C atoms in graphite-like structures. The D mode, which is forbidden in perfect graphite, is found at ~1350 cm^{-1} and becomes active only in the presence of disorder.[33] All recorded curves were fitted using Lorentzian lineshapes and the intensity ratios (namely, I_D/I_G) were calculated from the fitted total curve parameters.[33−35] According to the literature,[35] D- and G-peak intensities were used for the calculation of the I_D/I_G ratios and the related average defects distance (L_D). Here, we anticipate that an I_D/I_G ratio of 1.6 was found in the pristine-MWCNT material, while sensibly different values were calculated for the functionalized f_1-MWCNT, f_2-MWCNT, and f_{OH}-MWCNT samples.

Fourier transform infrared (FTIR) spectroscopy was performed on a Bruker FTIR Spectrometer (Mod. VERTEX-80 V) equipped with a broadband MCT detector that was cooled at liquid N_2 temperature. All CNT samples were prepared by mixing spectroscopic-grade KBr with MWCNTs or *f*-MWCNTs (2−3 wt %) and analyzed in the 400−4000 cm^{-1} range (800 scans) with a resolution of 1 cm^{-1}. X-ray powder diffraction (XRPD) measurements were carried out in a Bragg−Brentano geometry with a Panalytical X'PERT PRO powder diffractometer that was equipped with a W/Si graded parabolic mirror and a PIXcel solid-state detector. The diffractograms were recorded in the 10−80° 2θ region, operating with Cu Kα radiation (λ = 1.5418 Å). A 7.5-mm-height antiscatter slit was used on the diffracted beam. The 2θ step size was 0.0263°, with a counting time of 317 s/step. The measurements were carried out in air at ambient pressure and temperature. Elemental analyses were performed using a Thermo FlashEA 1112 Series CHNS-O elemental analyzer with an accepted tolerance of ±0.4 units. The Brunauer−Emmett−Teller (BET) specific surface area (SSA) and porosity (the latter based on *t*-plot methods) were measured on an ASAP 2020 Micromeritics instrument, using N_2 as absorbent at liquid N_2 temperature. Before measurements, all CNT samples (~30−40 mg) were completely degassed at 60 °C for 24 h. The temperature-programmed desorption (TPD) experiment for the MWCNT active surface area (ASA) determination was performed using a U-shaped quartz plug-flow reactor coupled with a Hyden Analytical HPR20 mass spectrometer that was equipped with a Selected ElectroMultiplier (SEM) detector for the analysis of volatiles (see the Supporting Information for procedure details).

1,3-Dipolar Cycloaddition of (*R*,*R*)-1, and (*S*)-2 onto MWCNTs. In a typical procedure, MWCNTs (120 mg) were weighed into a two-necked 250-mL flask and suspended in 58 mL of dry and degassed DMF. The suspension was sonicated for 15 min and then treated with a degassed DMF solution (2 mL) of nitrone **1** (360 mg, 1.56 mmol) or **2** (245 mg, 1.56 mmol). The mixture was maintained under vigorous stirring and under nitrogen atmosphere and heated at 160 °C for three days, then allowed to reach room temperature upon standing overnight. The suspension was filtered through a 100-nm-pore polycarbonate membrane and the solid residue was washed in sequence with dichloromethane (3 × 20 mL), water (3 × 20 mL), and ethanol (3 × 20 mL), each time being sonicated for 10 min and separated from the supernatant by centrifugation. The solid residue (~110−120 mg for both samples) was then dried under vacuum at 50 °C to constant weight to give functionalized MWCNT samples labeled as f_1-MWCNTs (those reacted with nitrone **1**) and f_2-MWCNTs (those reacted with nitrone **2**).

Preparation of f_{OH}-MWCNTs. In a typical procedure, f_1-MWCNTs (80 mg) were weighed into a 25-mL Schlenk flask and suspended in trifluoroacetic acid (10 mL). The suspension was degassed and sonicated for 15 min before maintaining it, at room temperature, under vigorous stirring and nitrogen atmosphere for 24 h. The mixture was then sonicated for 15 min and stirred at room temperature for an additional 24 h. The suspension was then filtered through a 100-nm-pore polycarbonate membrane and the solid residue was washed with an EtOH/H_2O mixture (1:1 v/v) (3 × 15 mL) and dried under vacuum at 50 °C to constant weight to give ~60 mg of the f_{OH}-MWCNT sample.

Preparation of the f_1-MWCNTs/PVPy Composites. The f_1-MWCNTs/PVPy nanocomposites were prepared by mixing aliquots [0.375 mL (0.5 wt %), 0.750 mL (1 wt %), 1.5 mL (2 wt %), and 2.25 mL (3 wt %)] of a freshly sonicated (1 h) stock DMF solution/dispersion of f_1-MWCNTs (4 mg/mL) with a hot DMF solution (60 °C) of poly(4-vinylpyridine) (PVPy, $\bar{M}_w \approx$ 160 000; conc: 300 mg/mL). After the mixture was stirred for 15 min, the nanocomposite thin films (dry film thickness of ~50 μm) were fabricated by casting the solutions on a glass Petri dish (Ø 7 cm) and evaporating to dryness in a fume hood at 40 °C overnight. Film detaching from the glass supports was obtained by heating under vacuum at 70 °C for 15−48 h.

Computational Methods. Calculations were performed on periodic models of CNTs of different morphologies (SWCNTs, MWCNTs, defected CNTs, etc.) with external diameters ranging from 4 Å to 15 Å. Supercells built by the replication of the nanotube unit cell from 4 to 6 times were taken into account in the model as to minimize spurious interactions between images of defect sites and/or chemisorbed species. Accordingly, periodic boundary conditions in three dimensions were applied, with a cell size in the direction parallel to the nanotube axis (*z*-axis) ranging from 15 Å to 25 Å and cell sizes in the other two dimensions large enough to keep a minimum distance of ~15 Å between system images. All calculations were performed at the spin-unrestricted DFT level by applying the PBE gradient-corrected exchange-correlation functional.[36] Reaction energies were computed as follows: $\Delta E = E_{\mathrm{ADDUCT}} - (E_{\mathrm{CNT}} + E_{\mathrm{NITRONE}})$, where E_{ADDUCT}, E_{CNT}, and E_{NITRONE} are the total DFT energies of the cycloaddition product, CNT and nitrone, respectively. Orbitals were expanded in terms of a localized basis set of double-ζ quality plus polarization with a plane-wave basis set for the expansion of the charge density with an energy cutoff of 200 Ry. Geometry optimizations were performed by relaxing all atomic degrees of freedom and the cell length in the *z*-direction until a maximum gradient of 0.02 eV/Å was obtained. A modified version of the Siesta program package[37,38] was used in all calculations.

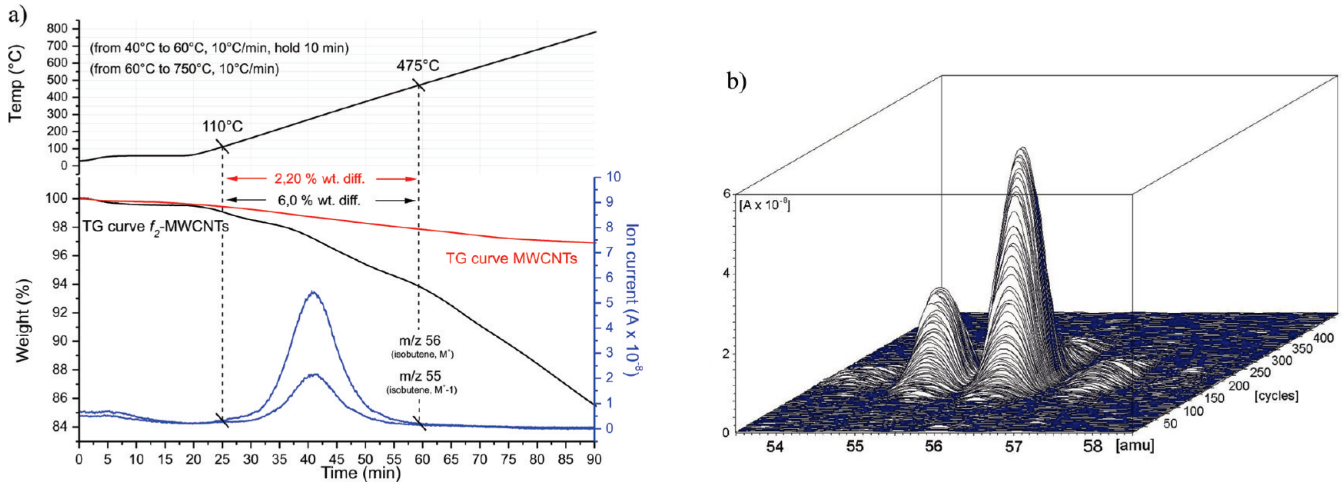

Figure 1. (a) TGA profiles of pristine MWCNTs and f_2-MWCNTs associated with the MS analysis of volatiles (N_2 atmosphere, 50 mL min^{-1}). (b) 3D representation of detectable mass peaks (m/z 55 and m/z 56) in the temperature range of 110−475 °C.

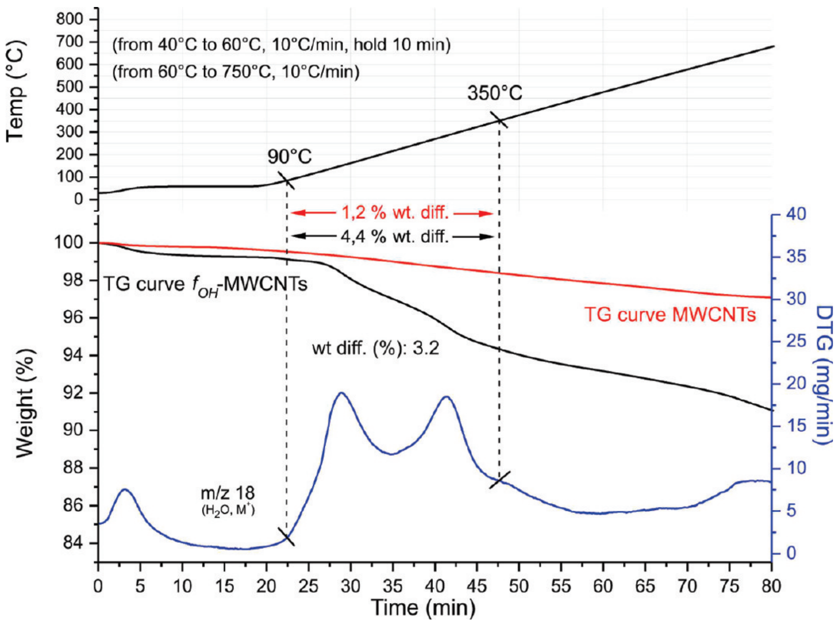

Figure 2. TGA profiles of pristine MWCNTs and f_{OH}-MWCNTs associated with the MS analysis (m/z 18) of volatiles (N_2 atmosphere, 50 mL min^{-1}).

RESULTS AND DISCUSSION

Nitrones are a class of 1,3-dipoles with large application in the synthesis of natural compounds and biologically active molecules.[39] In particular, the stereohomogeneous di-*tert*-butoxypyrroline *N*-oxide **1** and the mono-*tert*-butoxypyrrolidine *N*-oxide **2** (see Scheme 1) have emerged as easily accessible 1,3-dipoles from the chiral pool for the synthesis of optically active hydroxypyrrolidines and bicyclic azaheterocycles, such as pyrrolizidines and indolizidines.[40−42] Their good reactivity, even with sluggish dipolarophiles,[43,44] together with their excellent thermal stability, make these five-membered cyclic nitrones excellent candidates for organic functionalization at the CNTs sidewall. Moreover, the facile and stereoconservative deprotection of the ^{t}BuO groups at the cycloadduct moiety allows for a fine tuning of the lipophilic/hydrophilic character of the functionalized materials.

The reaction of nitrones **1** and **2** with MWCNTs was carried out under similar experimental conditions (solvent, reaction time, and temperature) and the final bulk functionalized materials (f_1-MWCNTs and f_2-MWCNTs) were used as-synthesized without further treatment. This chemistry produces a high functionalization degree and it can be easily performed on a relatively large scale. Evidence of the sidewall functionalization was first obtained by comparing the TGA profiles of f_1-MWCNTs and f_2-MWCNTs (Figure 1a) with those of the pristine MWCNTs. To make this comparison as truthfully as possible, the pristine sample was subjected to a similar thermal treatment (160 °C for three days)/sonication/washing/filtration workup of the functionalized materials, before being characterized. A mass analysis performed on the low-molecular-weight volatiles (from 25 amu to 125 amu), produced during the thermogravimetric tests (carried out under N_2 atmosphere), was used to obtain a qualitative information on the composition of the functionalized samples, together with an elucidation of the thermal decomposition path of the organic functional groups present at the CNT sidewall (see Figures 1a and 1b). Consistent with previously reported results on the f_1-MWCNT sample,[30] a weight loss of 3.80% was calculated for the f_2-MWCNTs in the temperature range of 110−475 °C (calculated as the weight difference between the TGA profiles of f_2-MWCNTs and pristine MWCNTs). Such a weight loss difference has been attributed to the thermal decomposition and rearrangement of the *tert*-butoxyl groups of the cycloadduct moieties, with isobutene evolution (m/z 56 M^+; m/z 55 $M^+ - 1$). A three-dimensional (3D) representation of the mass peaks observed accounts for the exclusive rearrangement of the *tert*-butoxyl groups to give isobutene (Figure 1b); no evidence of different decomposition paths or other significant mass fragmentations was obtained in the specific temperature range. At higher temperatures, only a gradual weight loss due to partial oxidative decomposition of the bulk material (m/z 44, CO_2 evolution) was observed. The lack of other relevant fragmentations led us to conclude that the MWCNT functionalization generates thermally stable chemical entities with both nitrones. This observation is consistent with the expected formation of hexahydro-pyrrole[1,2-*b*] isoxazole frameworks at the CNT sidewall. On the basis of the thermogravimetric profile, one may definitively conclude that a 10.6 wt % of the 3-^{t}BuO-nitrone **2** is grafted onto the MWCNT sidewalls, which roughly corresponds to one *tert*-butoxypyrrolidine *N*-oxide group every 110 C atoms. The N and O quantitative elemental analysis (pristine MWCNTs: N, 0.03; O, 0.00; f_2-MWCNTs: N, 0.72; O, 2.47) approximately refers to one *tert*-butoxypyrrolidine *N*-oxide group every 146 C atoms, in fairly good agreement with the loading previously calculated.

The higher functionalization degree for f_2-MWCNTs, compared to the previously reported di-*tert*-butoxypyrrolidine *N*-oxide-containing materials (f_1-MWCNTs),[30] can be ascribed to the higher reactivity of the less sterically crowded nitrone **2**. Nevertheless, f_2-MWCNTs showed a lesser extent of solubility/dispersibility in aprotic polar organic solvents (CH_2Cl_2, DMF), when compared to f_1-MWCNTs. Solutions with a maximum content of 3 mg of f_2-MWCNTs were prepared by rapid sonication of the functionalized CNTs in DMF to give stable inks with no apparent CNTs rebundling over a time period of weeks. On this ground, the unprecedented solubility observed for the previously reported f_1-MWCNTs in DMF (close to 10 mg of f_1-MWCNTs per mL of DMF) is probably due to higher solvation effects of the two dangling ^{t}BuO arms.

On the f_1-MWCNT sample, the deprotection of the ^{t}BuO groups at the cycloadduct moieties was achieved by treatment with trifluoroacetic acid at room temperature.[45,46] The thermogravimetric profile for the resulting f_{OH}-MWCNTs showed two distinct weight losses between 90 °C and 350 °C, which were assigned to the thermal decomposition of the hydroxy functionalities with water evolution (m/z 18, H_2O), while the initial slight weight variation (0.8%) was ascribed to the elimination of adsorbed humidity (Figure 2). Above 350 °C, a gradual weight loss, due to the partial decomposition of the CNT networks and residual organic fragments attached to their sidewalls (m/z 44, CO_2 evolution), was recorded. Finally, the complete deprotection of the *tert*-butoxyl groups was deduced from the disappearance of the typical isobutene mass fragmentation (m/z 55 and 56).

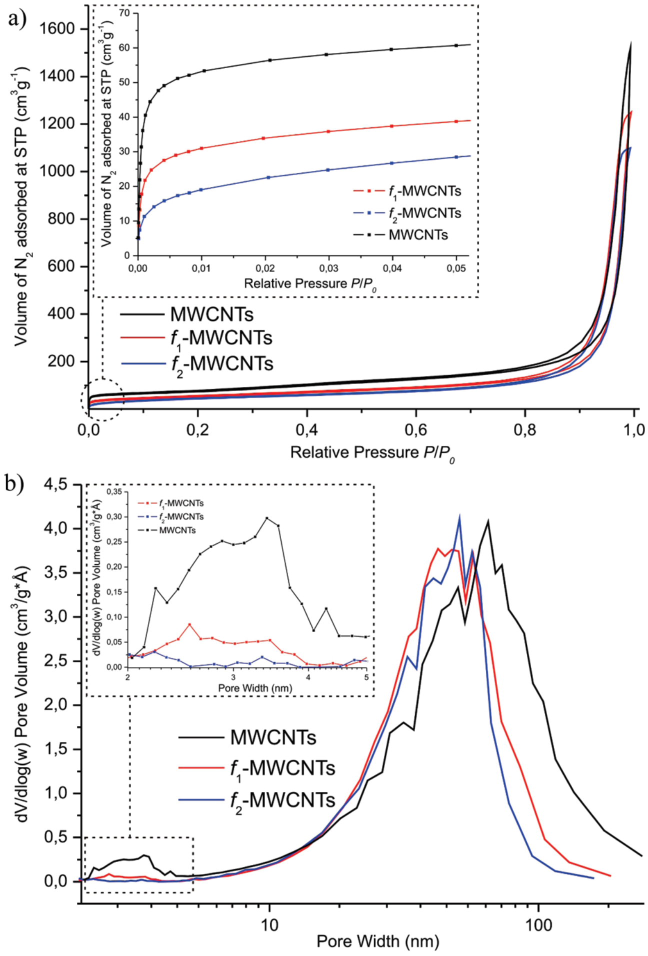

Figure 3. (a) Nitrogen adsorption−desorption isotherm linear plot (BET) of pristine and functionalized MWCNTs recorded at 77 K (inset involves the volume of N_2 adsorbed at partial pressures of $P/P_0 < 0.05$). (b) Pore volume distribution [$dV/d\log(w)$] for pristine and functionalized MWCNTs (inset involves the pore volume distribution in the micropore region).

Unlike the f_1-MWCNT and f_2-MWCNT samples, the dihydroxy-pyrrolidine *N*-oxide functionalized materials (f_{OH}) showed very modest solubility in either DMF or CH_2Cl_2 and CH_2Cl_2/EtOH (1:1) mixtures. Light-gray solutions of f_{OH}-MWCNTs (with no CNT rebundling upon standing for weeks) were prepared by sonication of the solid sample in the proper solvent with concentration spanning from 0.1 mg/mL to 0.15 mg/mL and 0.25 mg/mL in CH_2Cl_2, CH_2Cl_2/EtOH (1:1), and DMF, respectively. This set of data, which perfectly matches with the solubility values reported in the literature for similar materials,[47] highlights the primary role of the sterically crowded alkyl groups at the CNT sidewall to maintain a high solubility/dispersibility degree for these macromolecules in common organic solvents.

Specific Surface Area (SSA) and Pore Size Distribution of the Functionalized Materials. Figure 3a illustrates the nitrogen adsorption isotherms of pristine and functionalized f_1- and f_2-MWCNTs. According to the IUPAC classification, all nitrogen adsorption isotherms can be described as Type IV profiles with a characteristic H1 hysteresis loop generated by regularly shaped mesopores.[48] A higher N_2 adsorption, at low partial pressure (<0.05), in the isotherm of pristine MWCNTs indicates the

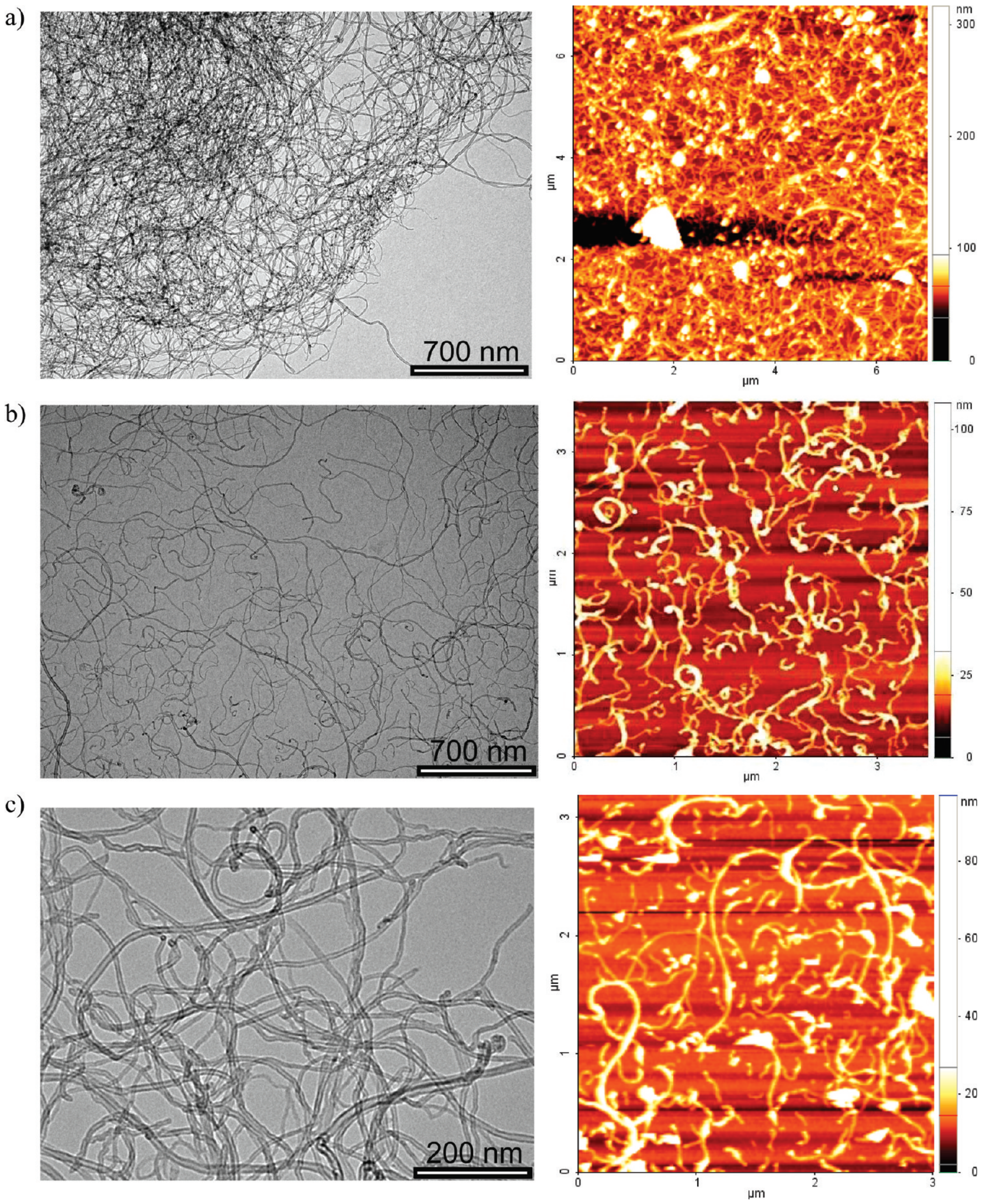

Figure 4. TEM (left) and AFM (right) images of (a) pristine MWCNTs, (b) f_2-MWCNTs, and (c) f_{OH}-MWCNTs. (For the morphological characterization of f_1-MWCNTs, see ref 30.)

presence of a higher micropore density in this sample, compared with the functionalized (f_1-MWCNT and f_2-MWCNT) materials (see inset of Figure 3a). Accordingly, the integrated areas enclosed within the limits $P/P_0 = 0-0.05$ showed a 3-fold decrease in the adsorbed N_2 volume, compared to the pristine sample, leading to a micropore volume decrease in the nitrone-functionalized materials. The measured specific surface areas (SSAs) are 263, 186, and 160 $m^2\ g^{-1}$ for pristine MWCNTs, f_1-MWCNTs, and f_2-MWCNTs, respectively.

The important decrease of the BET SSAs (up to 39%) in the functionalized samples is not totally unexpected,[49,50] yet it fits well with the observed micropore density reduction in the nitrone-functionalized materials (see Figure 3b and inset of the micropore region). Indeed, it has been well-established that nitrogen physisorption occurs not only on the exterior walls of CNTs but also in the void regions (channels and grooves) that exist between individual entangled nanotubes or nanotube bundles.[49,51]

In addition, the reduction of the SSAs and microporosity in the functionalized materials is ultimately a proof of their higher

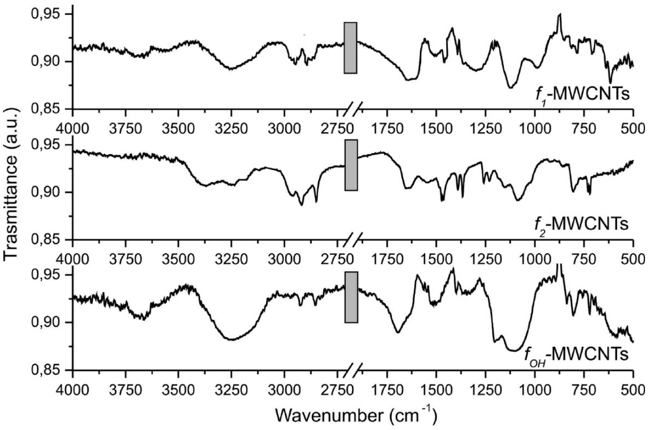

Figure 5. FT-IR spectra of (a) f_1-MWCNTs, (b) f_2-MWCNTs, and (c) f_{OH}-MWCNTs.

degree of deaggregation. Indeed, microporosity is mainly due to the presence of channels along with the CNT bundles.[49,52,53] Therefore, the nitrone functionalization of the CNTs sidewall is expected to reduce the supramolecular interactions responsible for the aggregation between the nanotubes also in the solid state.

Morphological, Spectroscopic, And Structural Characterization of the Nitrone-Functionalized MWCNT Samples. TEM and AFM characterization of the pristine and functionalized materials has provided evidence of the MWCNT-sidewall functionalization. A comparison of TEM and AFM images obtained for raw (Figure 4a) and functionalized (Figures 4b and 4c) materials clearly showed a high degree of deaggregation in solution for all the nitrone-treated samples. Although f_1-MWCNTs[30] and f_2-MWCNTs (Figure 4b) did not show any relevant morphological difference, revealing highly separated tubes throughout the entire observed area, small bundles of tubes were observed for the dihydroxypyrrolidine *N*-oxide derivatives (f_{OH}-MWCNT), in perfect agreement with their lower solubility/dispersibility (vide supra). For all the raw and functionalized nanomaterials studied, the nanotube lengths span from 100 nm to several micrometers, while the external diameters fall in the range of 10−30 nm. In both pristine and functionalized samples, neither appreciable changes of the MWCNT diameters and lengths nor the presence of amorphous material were observed.

Additional experimental characterization of the MWCNT functionalization was provided by the FTIR spectra of f_1-, f_2- and f_{OH}-MWCNT samples (see Figure 5).

Well-defined ν(C−H) and ν(C−O−C) vibrational modes between 2950−2750 cm^{-1} and 1120−1080 cm^{-1}, respectively, together with the $\delta(CH_2/CH_3)$ modes at 1470−1430 cm^{-1} and 1390−1365 cm^{-1}, appeared on the transmission profiles of both f_1- and f_2-MWCNTs. Reduced C−H stretching/bending intensities were observed in the f_{OH}-MWCNT sample, while a broad band between 3250 and 3500 cm^{-1} was assigned to the ν(O−H) modes.

Raman Spectroscopy, XRPD, and ASA Measurements. It is well-established that CNTs exist in many possible morphological variations, depending on the methods used for their preparation.[54−59] The knowledge and control of their final carbon texture and crystallite size distribution are of fundamental importance while studying their covalent or noncovalent sidewall functionalization.[54,55,59,60] While it might be possible to justify, on theoretical grounds, that CNTs with very small diameters (1−5 nm), such as SWCNTs, exhibit a chemical reactivity that is different from that of graphite, there is no fundamental reason why MWCNTs with diameters of >10 nm should behave differently, chemically speaking, from graphite.[61] To this purpose, "structural disorders" in MWCNTs related to different types of reticular imperfections at the graphitic lattice [Stone-Wales defects, vacancies and divacancies (Frenkel type pairs), edge-like defects, tube kinks, interstitial defects between external and internal tubes][62−64] are usually invoked to account for the large part of the chemical and electrochemical activity of these macromolecular systems.[30,55,59,61,65] The presence of low-organized carbon is also responsible for the high SSA and ASA values (see the Specific Surface Area (SSA) and Pore Size Distribution of the Functionalized Materials section). Raman spectroscopy investigation conducted on pristine and functionalized MWCNTs suggests that surface defect sites, particularly in the form of exposed edge-like defects and holes at the tube walls,[66] play a major role in the 1,3-dipolar cycloaddition of the cyclic nitrones under study to the MWCNT sidewall.

The Raman spectra of pristine and functionalized MWCNTs excited with the 514.5-nm laser line under inert atmosphere are shown in Figure 6. Typically, all spectra exhibit three main characteristic bands in the spectral region between 1000 and 2000 cm^{-1} (D, D′, and G modes), and their overtone and combination bands between 2400 and 3400 cm^{-1} (G′ = 2D). While the first-order G mode ($E_{2\,g}$ symmetry) is attributed to a regular sp^2 graphitic network, the D and D′ modes ($A_{1\,g}$ symmetry) are due to the so-called double resonant Raman scattering from a nonzero-center phonon mode, and they are originated from disorder and defects in the carbon lattice.[33,34,67−73] Finally, the radial breathing modes (ω_{RBM}) around 180−260 cm^{-1} are too weak to be observed, because of the large diameters of the sample tubes (10−30 nm). Accordingly, the intensity ratio between the D and G modes (I_D/I_G) is commonly used as a benchmark of the crystallite and defect sites surface density. From a closer examination of the spectra reported in Figure 6, it can be inferred that the functionalization process reduces the I_D/I_G intensity ratio, suggesting that a substantial modification occurs at the nanotube surface. As a matter of fact, the value of the intensity ratio observed in the pristine material ($I_D/I_G = 1.6$) reduces to 1.1 in all the functionalized MWCNTs [see panels (c), (d), and (e) in Figure 6, respectively]. Panels (a) and (b) refer to the same sample of pristine MWCNTs before and after the experimental/workup procedure, respectively (see the Experimental Section and General Considerations sections). Identical D- and G-mode intensities recorded for pristine and treated samples definitively exclude any appreciable chemical modification of the CNT surface in the absence of the functionalizing dipole (nitrone **1** or **2**), as well as any change in the D-band of the functionalized samples, [panel (b) vs panels (c) and (d)], because of the simple removal of the carbonaceous impurities.

These results indicate that the 1,3-dipolar cycloaddition of nitrones **1** and **2** does not occur at the lattice points of the regular sp^2 network but involves the diffuse Raman active defect sites at the CNT sidewall responsible for the D- and D′-mode intensities.[30,74] A phenomenological model to correlate the graphite defect density to the I_D/I_G ratio has been recently proposed by Lucchese and co-workers.[35] According to this model, the average distance L_D between the defects increases from 7.3 nm (treated MWCNTs) to 9.4 and 9.8 nm for f_1-MWCNTs and f_2-MWCNTs, respectively. The acid treatment for the *tert*-butoxyl deprotection at the f_1-MWCNT does not

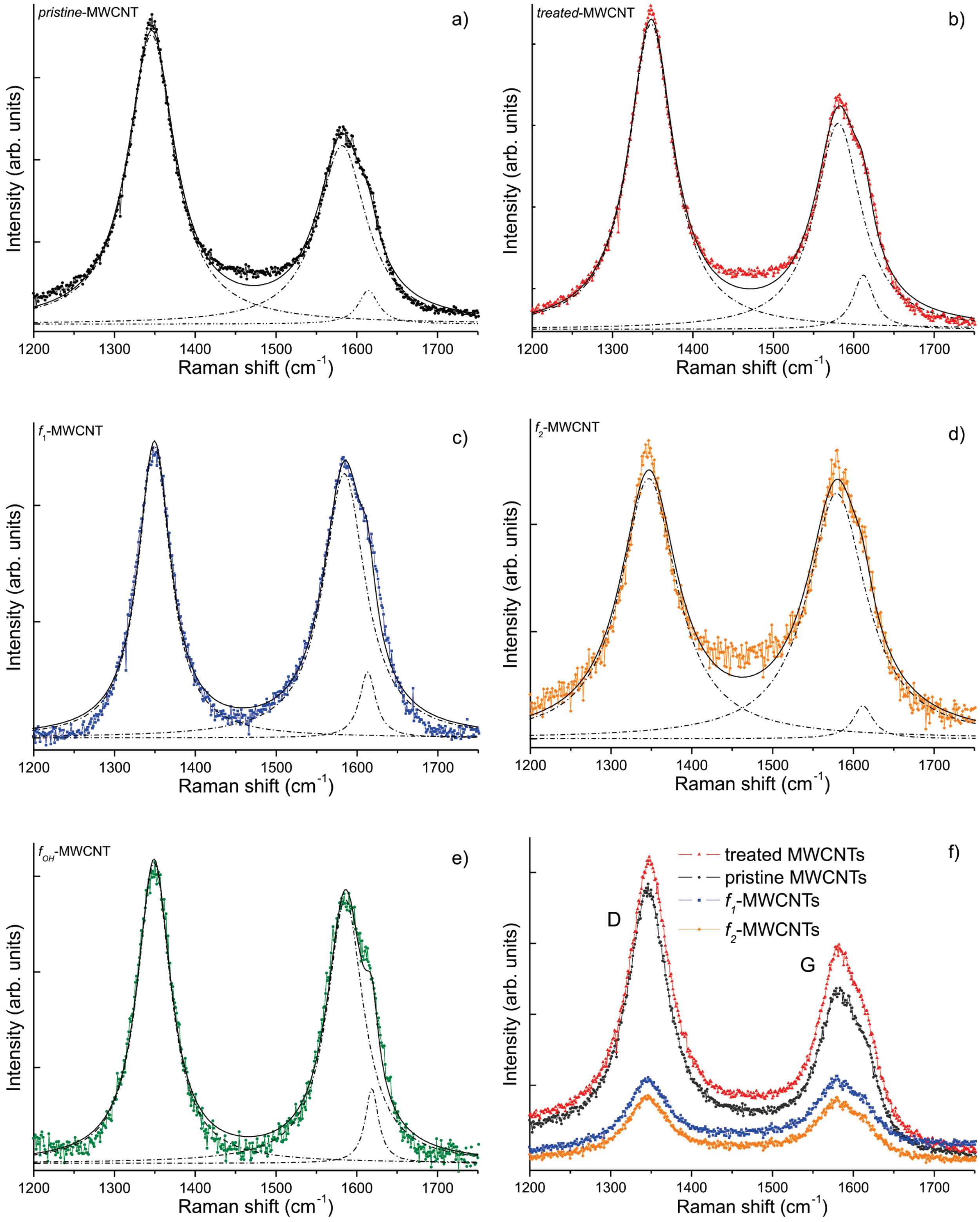

Figure 6. Raman spectra of (a) pristine, (b) treated, and (c, d, e) functionalized MWCNTs. The comparison among the various spectra (panel f) evidences that the functionalization process modifies the I_D/I_G ratio, suggesting that a surface modification has occurred. (The colored dots represent the experimental points. The single peak fittings are represented by dot-dashed lines, while the full line represents the total fit to the spectrum.)

produce any apparent modification in the I_D/I_G ratio of the f_{OH}-MWCNT sample, which translates into a roughly unchanged L_D value (9.3 nm). Finally, a G-peak downshift of ~4 cm^{-1} observed in the functionalized samples, with respect to both pristine and treated MWCNTs, accounts for nanotube surface modifications that ultimately decrease the intrabundle interactions. A similar downshift has been proposed for other covalent CNT functionalizations.[75,76] Finally, this result agrees with the observed SSA

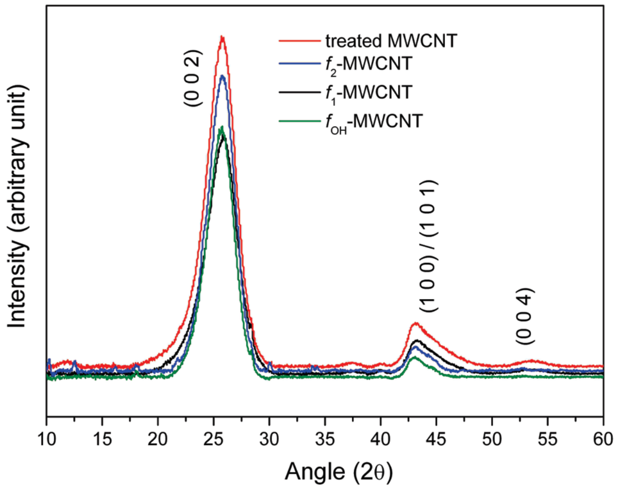

Figure 7. X-ray powder diffraction (XRPD) profiles [recorded in the 10°−80° 2θ region, operating with Cu Kα radiation ($\lambda = 1.5418$ Å)] of treated MWCNTs (red curve), f_1-MWCNTs (black curve), f_2-MWCNTs (blue curve), and f_{OH}-MWCNTs (green curve).

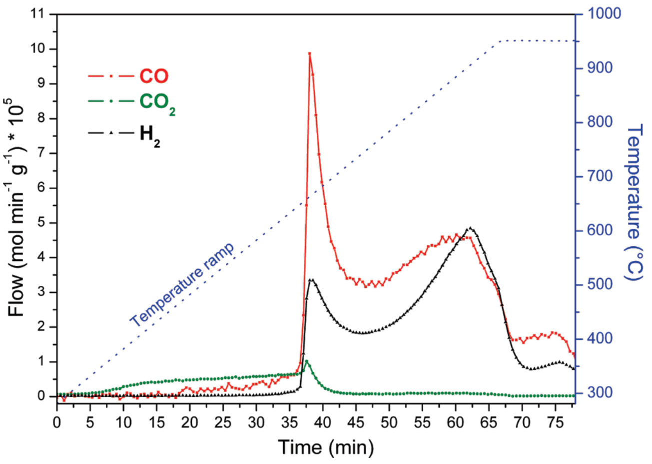

Figure 8. Temperature-programmed desorption (TPD) profile from MWCNT obtained after oxygen chemisorption at 300 °C.

decrease of the functionalized samples, because of the reduction of the void regions (micropore channels and grooves) existing between the individual entangled nanotubes.[49,51] (See the BET discussion in the Specific Surface Area (SSA) and Pore Size Distribution of the Functionalized Materials section.)

The knowledge and control of the CNT surface features is of mandatory importance when studying any type of covalent or noncovalent CNT sidewall functionalization. Two additional experiments, apparently complementary to the Raman scattering technique, were set up to characterize the CNT surface properties. First, XRPD diffractograms were acquired for CNT samples before and after the functionalization with nitrones **1** and **2**. Consistent with the Raman measurements, the XRPD diffractograms revealed that both crystallinity and morphology of the CNTs were preserved during the sidewall functionalization.[77,78]

No relevant shifts in the peaks position could be measured (Figure 7), while only negligible half-height peak-width (full width at half maximum, fwhm) variations were calculated for the different CNTs samples (f_1-MWCNTs, fwhm = 2.96°; f_2-MWCNTs, fwhm = 3.14°; f_{OH}-MWCNTs, fwhm = 3.07°; and pristine MWCNTs, fwhm = 3.16°). The Scherrer equation applied to these patterns revealed that the average number of ordered graphite layers in the crystallites of all the analyzed samples was constantly equal to eight (see the Supporting Information).[55]

Next, the surface properties of pristine MWCNTs were investigated with the concept of active surface area (ASA).[60,79−81] This technique allows for the evaluation of the chemically accessible and reactive sites present at the surface of carbon nanostructures, which are largely responsible for their chemical and electrochemical reactivity.[30,55,59,61,82] These reactive sites, usually located at the edge of the graphene planes as point defects, vacancies, and dislocations inside the hexagonal network,[60,83,84] are generally high-surface-energy sites and hence can be easily oxidized, generating carbon−oxygen surface groups. On these grounds, the ASA value was quantified using an oxygen chemisorption experiment, followed by analysis of the composition of the gas evolved during a temperature-programmed desorption (TPD) experiment. As shown in Figure 8, during the TPD experiment, the evolution of significant quantities of CO and H_2, and a small amout of CO_2, was clearly observed. The latter is observed between 350 °C and 700 °C, while CO and H_2 evolution could be detected at temperatures over 650 °C, with similar profiles in the entire scanned temperature range. The amount of CO and CO_2 desorbed was used for the ASA calculation. The integration of the CO and CO_2 traces accounts for $\sim 8.1 \times 10^{-4}$ mol C/g_{MWCNT}, which is consistent with a relatively high ASA value of ~ 12.8 m^2/g_{MWCNT} that is potentially available for the covalent bonding.[82]

This ASA value represents 4.8% of the total surface area measured by N_2 physisorption (SSA), a fraction that is in good agreement with the ASA and SSA values reported in the literature for commercially available MWCNT samples.[60]

Theoretical Calculations. Understanding the role of topological defects on the covalent functionalization of complex carbon nanostructures (such as the MWCNTs used herein) is an important prerequisite to gain insight into their chemical reactivity. Moreover, the way nitrones graft to the MWCNT sidewalls may be used to account for other related organic functionalizations with different 1,3-dipoles.[47] While the electrochemical activity of defect-containing CNTs has been intensively investigated,[54,55,61] equal attention has not been devoted to unveil the role of "disordered carbon" (nongraphitic active sites and domains) at the outer sidewall network of MWCNTs, with respect to their chemical reactivity[55] in cycloaddition reactions. Unravelling the operative mechanisms responsible for the reactivity of **1** and **2** on complex and disordered carbon nanostructures such as MWCNTs is certainly beyond the scope of the present study. On the other hand, DFT calculations on the reactivity of selected topological defects at the CNT sidewalls can be used to trace-out a "defect-based" sidewall reactivity trend. This aspect is of major importance for the organic functionalization of macromolecular structures with a diameter larger than 10 nm (such as MWCNTs), since their reduced external curvature, when compared to other carbon nanostructures such as SWCNTs and fullerenes, would decrease the chemical reactivity of the sp^2 sidewall. The interplay between the electronic structure of the reactive site and its high defect-induced surface energy (due to C−C bond reconstructions and local deformations) is the key factor to be taken into account for the analysis of the nitrones cycloaddition reaction.

Table 1. Summary of the ΔE Values [kcal (mol)$^{-1}$] for the 1 and 2 Cycloaddition Reaction to Carbon Nanostructures[a]

nitrone	(18,0)	(5,5)	(18,0) Stone-Wales	(9,0)//(18,0) 5−1DB	(9,0)//(18,0) double vacancy	armchair GNR	armchair GNR (−COOH)	zigzag GNR	C_2H_4	C_{60} [6,6]	graphene
1	+22.8	+2.2	−0.9	unstable	−43.9	+2.4	−6.0	unstable	−28.1	−15.8	+17.5
2					−39.4		−6.0		−28.4	−13.8	

[a] Calculated energies for the cycloaddition reaction occurring on ethylene (C_2H_4), fullerene (C_{60}), and graphene have been reported for comparison.

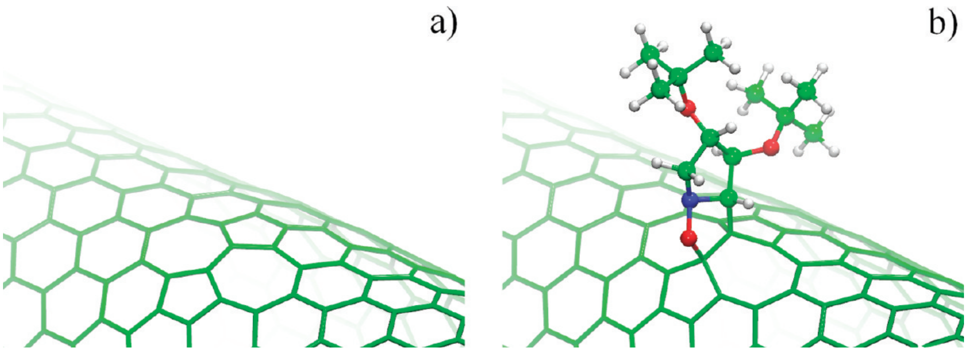

Figure 9. (a) Optimized structure for a SW defect on the sidewall of a (18,0) SWCNT; (b) optimized structure for nitrone **1** interacting with the defect site shown in panel a.

Preliminary DFT calculations for the CNT cycloaddition of nitrone **1** have been conducted on a defect-free sidewall of a zigzag (18,0) and an armchair (5,5) SWCNT, respectively. In particular, we have considered the reaction of **1** on the transversal and circumferential C−C bonds at the sidewalls, typically recognized as the most chemically reactive sites.[85] SWCNTs have been selected as CNT models, since the weak dispersion forces existing among adjacent walls in a MWCNT do not affect the chemical properties of its defect-free outer sidewall.[86]

In agreement with previously reported theoretical studies on similar 1,3-dipole-CNT cycloadditions,[19,87−89] the computed energies for the reaction of **1** with defect-free sidewalls were thermodynamically unfavored [+22.8 kcal mol^{-1} for a zigzag (18,0) and +2.2 kcal mol^{-1} for an armchair (5,5) SWCNT; see Table 1].

Note that the outer diameters of both SWCNTs taken into account [(18,0) ≈ 1.4 nm, (5,5) ≈ 0.7 nm)] are 10−20 times smaller than the average diameter of the MWCNTs used in our experiments (Ø ≈ 15 nm). In view of the typical CNT reactivity decrease for increasing diameters,[27] one may infer that the same cycloaddition reaction carried out on a larger diameter defect-free sidewall will be even less favored.

Turning the attention to the analysis of the CNT defects as higher surface energy sites for covalent bonding, the Stone-Wales (SW) defects generated from the displacement of one C atom between two adjacent C_6-rings, was first examined as one of the most common topological defects present in the real CNT samples.[90] Previous works indicate that these defects are more reactive sites than the defect-free hexagonal C-atom networks.[91,92] In particular, the SW defects originated from the rotation of a C−C bond that is parallel to the axis of a zigzag CNT (Figure 9a) usually exhibit a larger propensity to functionalization.[93] On these grounds, we have evaluated the reaction energy for the cycloaddition of **1** to the latter type SW defect originated on a (18,0) SWCNT (see Figure 9b).

As for defect-free systems, the interactions between an outer nanotube sidewall containing a SW defect and the inner tubes (as for the case of a MWCNT) can be considered negligible. Calculations revealed that the cycloaddition reaction is thermodynamically favored, compared to the cycloaddition onto a defect-free sidewall, but it is basically thermoneutral (−0.9 kcal mol^{-1}). Although the small reaction energy computed for the cycloaddition of **1** to this topological defect cannot be invoked to justify the high degree of functionalization experimentally observed in MWCNTs, the comparison with a defect-free system certainly strengthens the idea of a defect-based reactivity trend.[91]

Hence, we focused our attention on the reactivity of **1** toward other common structural defects present at the CNT sidewalls, such as single vacancies (SVs) and double vacancies (DVs). The former, which originates from the removal of a single C atom from the hexagonal network of the sidewall, can be generated either by specific CNT growth techniques[94] or by electron-beam irradiation.[95] The removal of a single C atom from the CNT sidewall causes a bond reconstruction/rearrangement in close proximity of the vacancy,[96] giving rise to new C−C bonds with enhanced reactivity.[97,98] A similar behavior is also predicted for DVs, where a favorable rearrangement of the π-electrons in the network[99] makes this type of topological defect remarkably more stable than the previous one.[99−101] In particular, the configuration constituted by two SVs, one for each adjacent coaxial graphitic shell, has been found to be thermodynamically stable and relatively common in defected MWCNTs.[102] Note that the strong electronic structure rearrangement induced by SVs or DVs can lead to an enhancement of MWCNTs interwall interactions; a direct consequence of this rearrangement is the improvement of the mechanical properties of multilayered carbon nanostructures.[103,104]

The reactivity of **1** onto SVs and DVs was assessed by calculations on systems obtained relaxing a periodic model structure for a (9,0)//(18,0) DWCNT, containing a total of 432 carbon atoms in the supercell, after removal of one or two C atoms, respectively. The combination of these two diameters sets the final interwall distance to 3.4 Å (a value that is almost identical to that

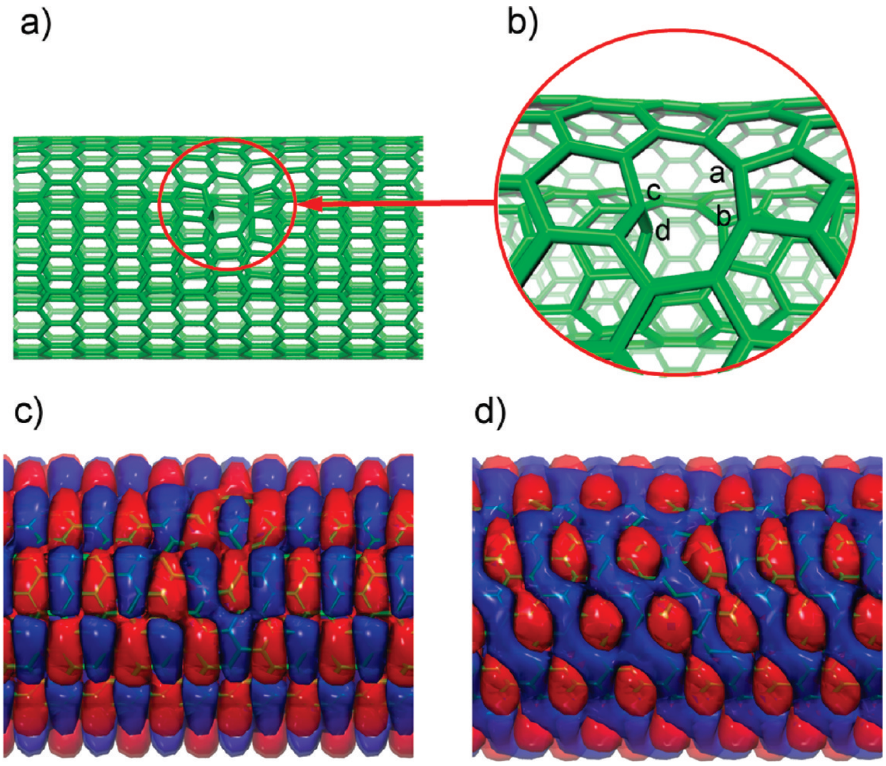

Figure 10. (a,b) Optimized structure and frontier orbitals [(c) HOMO and (d) LUMO] for a (9,0)//(18,0) DWCNT with a reconstructed double vacancy (DV) in the "interlinked" configuration.

found in graphite), thus maximizing the attractive π-stacking interaction between the tubes.[105] Accordingly, in the computational model a SV originated from the removal of one C atom from the outer (18,0) nanotube shell and a DV originated from the removal of two C atoms from adjacent shells of a (9,0)//(18,0) DWCNT were taken into account.

The most stable configuration for a SV corresponds to the 5−1DB defect, commonly observed in SWCNTs (see Figure S1 in the Supporting Information).[96,97] However, DFT calculations concerning the cycloaddition of **1** to different C−C bonds in the proximity of the 5−1DB defect site did not show any evidence of formation of stable chemically bound adducts (Table 1). This behavior can be ascribed to the peculiar electronic structure of a SV, which is known to delocalize the spin-polarized electron density over the conjugated π-electron skeleton.[96] As a result, radical reactions are strongly favored at this vacancy,[97] while only a negligible contribution to the 1,3-dipolar nitrone cycloaddition at the C−C sites is expected.

In the DV case, the model system generated by the removal of two adjacent C atoms from both sidewalls of a (9,0)//(18,0) DWCNT resulted in, upon reconstruction, a stable energy minimum, corresponding to an "interlinked" configuration (Figure 10a and 10b).[64,103] Notably, the frontier orbitals of this geometry (Figures 10c and 10d) are very similar to those of a pristine SWCNT; this indicates a minor effect on the overall electronic properties of the reconstructed DV-defected sidewall. Moreover, the final electronic structure exhibits a marked singlet-spin closed-shell character, as expected for rearrangements of the electronic configuration that permit the recovery of the sp^2 hybridization of the C atoms.[106−108]

The addition of **1** to the most accessible of the C−C bonds in the proximity of the defect results in unstable products. However, the addition of **1** to the C−C bond of the reconstructed pentagonal ring and perpendicular to the nanotube axis (bond C_a−C_b in Figure 10b), leads to a stable adduct, shown in Figure 11, which is 43.9 kcal mol^{-1} more stable than the reagents, suggesting a remarkable reactivity of the DV with respect to the cases previously discussed. Note that the reaction proceeds by breaking the C−C bond where the cycloaddition takes place. This effect, previously observed for other CNT sidewall reactions involving strained C−C bonds, is partially responsible for the enhanced reactivity in the cycloaddition reaction of **1**.[109]

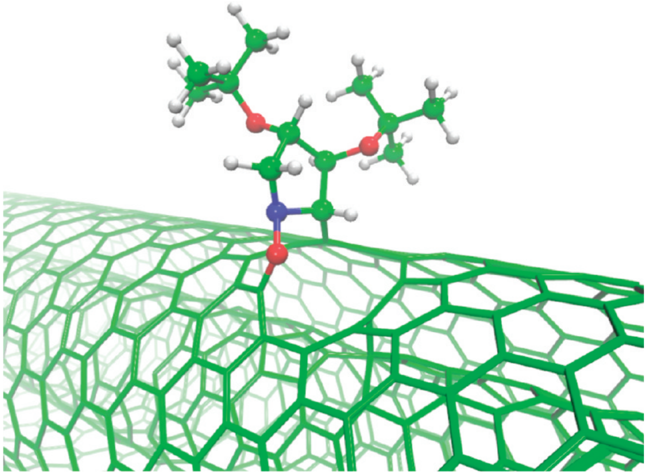

Figure 11. Optimized structure for the product of the addition of nitrone **1** to the site originating from a DV on a (9,0)//(18,0) CNT. Atom colors are coded as follows: green, carbon; red, oxygen; white, hydrogen; and blue, nitrogen.

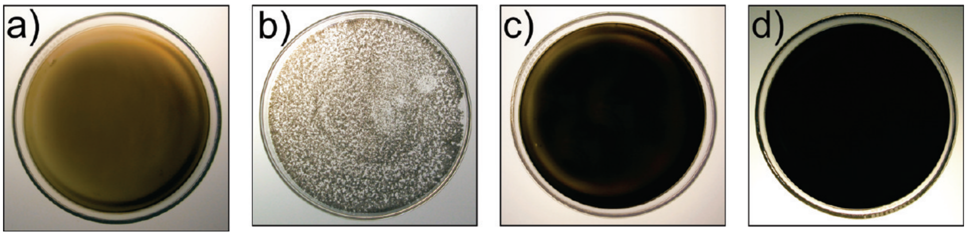

Figure 12. PVPy-f_1-MWCNT composites at variable nanofiller loadings: (a) 0.5 wt %; (c) 1 wt %, and (d) 3 wt %. Panel b shows a sample prepared with a 0.5 wt % loading of pristine MWCNTs.

Finally, the presence of edge-like defects at the CNT sidewalls was considered by computing the energy for the cycloaddition of **1** to the edges (armchair or zigzag) of graphene nanoribbons (GNRs).[110] Indeed, the morphology of the edge-like defects exhibits marked structural similarities with the GNR edges.[55] In particular, we considered the addition of **1** to the terminal C−C bonds, parallel and transversal, with respect to the GNR axis for armchair and zigzag edges, respectively (see Figures S2 and S3 in the Supporting Information). These C−C bonds are commonly recognized as the most reactive attack sites for GNRs.[110] The reaction of **1** with both types of edge-like defects gave unfavorable cycloaddition energies. While a slightly endothermic process was calculated in the case of an armchair edge defect (2.4 kcal mol^{-1}), calculations for the zigzag-type edge defect only led to a weakly bound adduct. Noteworthy, the calculations carried out on oxidized edge-like defects, modeled through the addition of a −COOH group to one of the carbon atoms of the π(C═C) reactive site at the armchair GNR (Figure S4 in the Supporting Information), led to a moderately favored thermodynamic process, passing from +2.4 kcal mol^{-1} to −6.0 kcal mol^{-1} (see Table 1).

Energy calculations carried out on the cycloaddition of **2** gave comparable results, without revealing any significant contribution from the reduced dipole steric hindrance; the relative reaction energies (for exoenergetic processes, with respect to the addition of nitrone **1**) are listed in Table 1.

In conclusion, the very high binding energy calculated for the cycloaddition of **1** to a DV of a DWCNT suggests that a closed-shell configuration of the sidewall, together with local distortions of the C−C bonds, may facilitate the overall process. These results are in agreement with the experimental arguments.[88,106−108]

f-MWCNTs/Poly-4-vinylpyridine Composites. Nanocomposite materials based on nanoscale-reinforced polymers represent an ever-increasing area of research.[5−10,111] It has been established that the combination of a soft polymer matrix with nanosized rigid filler particles can provide new composite materials with largely improved modulus and strength, even at very low nanofiller loadings.[112−114] On this ground, the unique mechanical, thermal, and electrical properties of carbon nanotubes, together with their very high aspect ratio, make these nanodimensional fillers among the best candidates for the preparation of polymer-reinforced nanocomposites with remarkable chemical and physical properties.[113] Notwithstanding, the successful usage of CNTs in polymer composites usually requires either a noncovalent or a covalent modification of the CNTs to improve their dispersibility/processability in both liquids and solid matrices, avoiding severe phase-segregation problems.[27,115−121] Although the organic functionalization of the CNT surface (covalent modification) represents a well-established approach to reach a high level of nanotube dissociation, its use in the preparation of CNT/polymer composites is a sort of double-edge sword. In fact, the higher the sidewall organic functionalization extent, the higher the corruption of the tube structural integrity with subsequent worsening of its mechanical properties.[122] At variance with other organic functionalization approaches, our method to increase the MWCNTs dispersibility provides highly soluble materials without affecting the crystal domain size of the sp^2 CNT network (see the Raman Spectroscopy, XRPD, and ASA Measurements section). Since the diffuse structural defects present on the MWCNTs act as preferential reactive sites, the physical and chemical properties of the original macromolecular fillers are preserved.

Poly(4-vinylpyridine) (PVPy) is an amorphous hydrophobic polymer with good solubility in aprotic polar solvents and excellent processability, both in solution and in the melt, to give freestanding thin films with several applications.[116,118,123] Because of the superior solubility of the f_1-MWCNT sample in DMF (compared with f_2- and f_{OH}-nanomaterials), it was the filler of choice in the preparation of PVPy-based composites at different CNT loadings. A PVPy solution in DMF was mixed with a DMF solution of f_1-MWCNTs (0.5−3 wt %) and the resulting mixture sonicated for 30 min before casting it on a 6-cm-diameter glass capsule (the initial thickness of the solution-cast samples in the present study was higher than 300 μm). Thereafter, the casting sample was allowed to evaporate under a fume hood at room temperature overnight and it was further dried to constant weight under high vacuum (ca. 10^{-6} bar) at 70 °C for 24 h. The same procedure was also applied to the preparation of a PVPy-based composite using 0.5 wt % of pristine MWCNTs. In contrast to the latter, where phase segregation effects were clearly visible (Figure 12b), PVPy composites prepared using f_1-MWCNTs showed a perfect and uniform dispersion of the nitrone-functionalized nanofillers to give either slightly gray and optically transparent films at lower nanofiller loadings (0.5−1 wt %; see Figures 12a and 12c) or uniformly dark and homogeneous polymer composites at higher nanofiller loadings (1−3 wt %; see Figure 12d).

All the composites prepared by the casting evaporative technique gave rise to thin films with thicknesses ranging from 45 μm to 55 μm that could be easily detached from the glass support upon standing under vacuum at 70 °C.

TEM analyses on the composites obtained using f_1-MWCNTs and pristine MWCNTs were carried out to address the influence of the CNT functionalization on the homogeneous dispersion of the nanofillers within the host PVPy matrix. Figures 13a, 13b, and 13c show three micrographs taken at different magnifications for the composites containing 0.5 wt % of pristine MWCNTs, 1 wt %, and 2 wt % of f_1-MWCNTs, respectively.

From these pictures, it is evident that the pristine nanotubes are poorly dispersed and not homogeneously distributed within

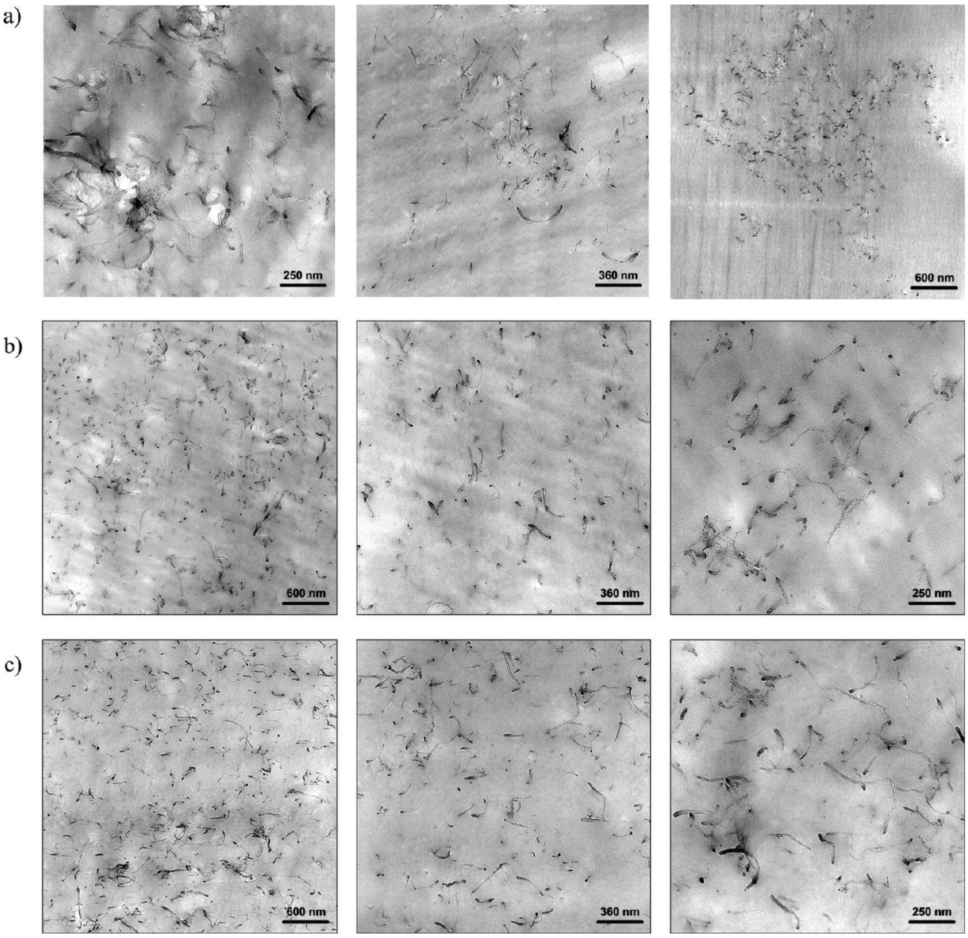

Figure 13. TEM micrographs of (a) PVPy-MWCNT composite at 0.5 wt % loading of pristine CNTs; (b) PVPy-f_1-MWCNT composite at 1 wt % nanofiller loading; (c) PVPy-f_1-MWCNT composite at 2 wt % nanofiller loading. From left to right micrographs are reported at increasing magnifications (12 000×, 20 000×, and 30 000×).

the polymer matrix (Figure 13a). Loosed micrometric bundles of nanotubes are present, together with a few single particles spread over the observed area. In contrast, the functionalization of MWCNT remarkably improves the filler distribution and dispersion. Indeed, in both cases where the f_1-MWCNT filler was employed, no micrometric bundles were anymore present, and only individual MWCNTs uniformly dispersed within the polymer matrix were observed, as shown in the TEM micrographs taken at different magnifications (see Figures 13b and 13c). Finally, the increased CNT loading was not found to reduce the overall fillers dispersion extent within the host PVPy matrix (see Figure 13b vs Figure 13c).

Differential scanning calorimetry (DSC) measurements conducted on each composite revealed only slight variations of the glass-transition (T_g) values, with respect to the neat PVPy film. Indeed, both composites prepared with pristine and functionalized MWCNTs showed T_g values comparable to that measured for pure PVPy; slight T_g changes were attributed to both the degree of dispersion and nanofillers loading. In particular, the slight increment (~1 °C) in the T_g value measured for the composite prepared with 0.5 wt % pristine MWCNTs is reasonably due to the presence of nanofillers not dispersed at a nanoscale level, as shown by TEM micrographs (Figure 13a). In contrast, a slight decrease of T_g values for the composites prepared with f_1-MWCNTs suggested the presence of an effective polymer/CNT interfacial interaction, improved by the MW sidewall-grafted functionalities and proved by the excellent dispersion/deaggregation degree of the nanofillers within the polymer. TGA profiles for PVPy and CNT-composites showed slightly improved termical properties with T_g^{onset} and midpoint temperatures up to 5 °C higher that those measured for the neat PVPy film[124,125] (see the Supporting Information).

■ CONCLUSIONS

Starting from curiosity-driven research ("Can nitrones functionalize carbon nanotubes?"),[30] the authors of this paper have been able to unveil the central role played by the lattice sidewall defects of complex carbon nanostructures (such as MWCNTs) on their covalent functionalization. The cyclic nitrones used in this study lead to the production of highly functionalized materials with unprecedented solubility/dispersibility in organic solvents. An in-depth surface chemical and spectroscopical analysis of the functionalized materials led to the conclusion that the sidewall structural defects present on the pristine MWCNTs act as preferential reactive sites for the nitrone 1,3-dipolar cycloaddition. The application of a phenomenological model capable of correlating the lattice defects density to the Raman I_D/I_G ratio has shown an increase of the average distance of Raman active defect sites while moving from pristine to functionalized samples. An interplay between the electronic structure of the reactive sites and their high defect-induced surface energy has been taken into account to calculate the thermodynamics associated to the nitrone cycloaddition to selected CNT topological defects.

Besides an unprecedented handling of modified MWCNTs, which paves the way to their convenient use in a wide number of applications (including the preparation of inks and nanocomposites), the key feature of the present functionalization approach (over others) involves its nondamaging character; indeed, the preservation of the CNT sidewall sp^2 network does not change the chemico-physical properties of the pristine materials.[126] In this respect, the nitrone-MWCNT covalent functionalization can be a valuable alternative to the noncovalent bonding approaches[11,127] for the generation of highly soluble/dispersible CNTs. Moreover, the way in which the nitrones graft to the MWCNT sidewalls may also contribute to elucidate other related organic functionalizations.[47]

Last, but not least, the facile chemical modification of the functional groups at the edge of the chiral pyrrolidine frameworks allows for a modulation of the hydrophobic/hydrophilic nature of the cycloaddition products. The introduction of chiral and tunable functional groups on the CNT sidewalls represents a starting point for the development of further nanotubes derivatization approaches.

■ ASSOCIATED CONTENT

Ⓢ Supporting Information. Details on the ASA measurements, Scherrer equation, BET surface areas. Optimized structures for a defective (9,0)//(18,0) CNT, armchair and zigzag graphene nanoribbon are also provided. Details of DSC measurements and TGA profiles for pristine and functionalized MWCNTs. (PDF) This material is available free of charge via the Internet at http://pubs.acs.org.

■ AUTHOR INFORMATION

Corresponding Author

*E-mails: giuliano.giambastiani@iccom.cnr.it, stefano.cicchi@unifi.it.

■ ACKNOWLEDGMENT

The authors thank the NANOCELL project (PAR FAS REGIONE TOSCANA Linea di Azione 1.1.a.3) for financial support to this work. Thanks are also due to the Ministero dell'Istruzione, dell'Università e della Ricerca (MIUR) and the GDRE network for support.

■ REFERENCES

(1) Iijima, S. *Nature* **1991**, *354*, 56.
(2) Monthioux, M.; Kuznetsov, V. *Carbon* **2006**, *44*, 1621.
(3) Ajayan, P. M. *Chem. Rev.* **1999**, *99*, 1787.
(4) Baughman, R. H.; Zakhidov, A. A.; de Heer, W. A. *Science* **2002**, *297*, 787.
(5) Jeevananda, T.; Siddaramaiah; Su Lee, T.; Hee Lee, J.; Samir, O. M.; Somashekar, R. *J. Appl. Polym. Sci.* **2008**, *109*, 200.
(6) Kashiwagi, T.; Grulke, E.; Hilding, J.; Harris, R.; Awad, W.; Douglas, J. *Macromol. Rapid Commun.* **2002**, *23*, 761.
(7) Kuan, C. F.; Chen, W. J.; Li, Y. L.; Chen, C. H.; Kuan, H. C.; Chiang, C. L. *J. Phys. Chem. Solids* **2010**, *71*, 539.
(8) Byrne, M. T.; Cun'ko, Y. K. *Adv. Mater.* **2010**, *22*, 1672.
(9) Park, S. H.; Bandaru, P. R. *Polymer* **2010**, *51*, 5071.
(10) Sahoo, N. G.; Rana, S.; Cho, J. W.; Lin, Li, L.; Chan, S. H. *Prog. Polym. Sci.* **2010**, *35*, 837.
(11) Karousis, N.; Tagmatarchis, N.; Tasis, D. *Chem. Rev.* **2010**, *110*, 5366.
(12) Tasis, D.; Tagmatarchis, N.; Bianco, A.; Prato, M. *Chem. Rev.* **2006**, *106*, 1105.
(13) Holzinger, M.; Abraham, J.; Whelan, P.; Graupner, R.; Ley, L.; Hennrich, F.; Kappes, M.; Hirsch, A. *J. Am. Chem. Soc.* **2003**, *125*, 8566.
(14) Holzinger, M.; Vostrowsky, O.; Hirsch, A.; Hennrich, F.; Kappes, M.; Weiss, R.; Jellen, F. *Angew. Chem., Int. Ed.* **2001**, *40*, 4002.
(15) Bahr, J. L.; Yang, J.; Kosynkin, D. V.; Bronikowski, M. J.; Smalley, R. E.; Tour, J. M. *J. Am. Chem. Soc.* **2001**, *123*, 6536.
(16) Coleman, K. S.; Bailey, S. R.; Fogden, S.; Green, M. L. H. *J. Am. Chem. Soc.* **2003**, *125*, 8722.
(17) Umek, P.; Seo, J. W.; Hernadi, K.; Mrzel, A.; Pechy, P.; Mihailovic, D. D.; Forro, L. *Chem. Mater.* **2003**, *15*, 4751.
(18) Padwa, A.; Pearson, W. H. *Synthetic Applications of 1,3-Dipolar Cycloaddition Chemistry Toward Heterocycles and Natural Products*; Wiley: New York, 2002.
(19) Lu, X.; Tian, F.; Xu, X.; Wang, N.; Zhang, Q. *J. Am. Chem. Soc.* **2003**, *125*, 10459.
(20) Lu, X.; Zhang, L.; Xu, X.; Wang, N.; Zhang, Q. *J. Phys. Chem. B* **2002**, *106*, 2136.
(21) Alvaro, M.; Atienzar, P.; de la Cruz, P.; Delgado, J. L.; Garcia, H.; Langa, F. *J. Phys. Chem. B* **2004**, *108*, 12691.
(22) Georgakilas, V.; Kordatos, K.; Prato, M.; Guldi, D. M.; Holzinger, M.; Hirsch, A. *J. Am. Chem. Soc.* **2002**, *124*, 760.
(23) Tagmatarchis, N.; Prato, M. *J. Mater. Chem.* **2004**, *14*, 437.
(24) Wang, N.; Iqbal, Z.; Mitra, S. *Carbon* **2005**, *43*, 1015.
(25) Chen, Z. F.; Thiel, W.; Hirsch, A. *ChemPhysChem* **2003**, *4*, 93.
(26) Gulseren, O.; Yildirim, T.; Ciraci, S. *Phys. Rev. Lett.* **2001**, *87*, 6802.
(27) Niyogi, S.; Hamon, A.; Hu, H.; Zhao, B.; Bhowmik, P.; Sen, R.; Itkis, M. E.; Haddon, R. C. *Acc. Chem. Res.* **2002**, *35*, 1105.
(28) Tada, K.; Furuya, S.; Watanabe, K. *Phys. Rev. B* **2001**, *63*, 5404.
(29) Cicchi, S.; Hold, I.; Brandi, A. *J. Org. Chem.* **1993**, *58*, 5274.
(30) Ghini, G.; Luconi, L.; Rossin, A.; Bianchini, C.; Giambastiani, G.; Cicchi, S.; Lascialfari, L.; Brandi, A.; Giannasi, A. *Chem. Commun.* **2010**, *46*, 252.
(31) Perrin, D. D.; Armarego, W. L. F.; Perrin, D. R. *Purification of Laboratory Chemicals*, 2nd ed.; Pergamon Press: New York, 1980; Vol. 1.
(32) Giannasi, A.; Celli, M.; Grazzi, F.; Ulivi, L.; Zoppi, M. *Rev. Sci. Instrum.* **2008**, *79*, 013105.
(33) Ferrari, A. C.; Robertson, J. *Phys. Rev. B* **2000**, *61*, 14095.
(34) Ferrari, A. C.; Robertson, J. *Phys. Rev. B* **2001**, *64*, 075414.
(35) Lucchese, M. M.; Stavale, F.; Martins Ferreira, E. H.; Vilani, C.; Moutinho, M. V. O.; Capaz, R. B.; Achete, C. A.; Jorio, A. *Carbon* **2010**, *48*, 1592.
(36) Perdew, J. P.; Burke, K.; Ernzerhof, M. *Phys. Rev. Lett.* **1996**, *77*, 3865.
(37) Artacho, E.; Sanchez-Portal, D.; Ordejon, P.; Garcia, A.; Soler, J. M. *Phys. Status Solidi B* **1999**, *215*, 809.
(38) Soler, J. M.; Artacho, E.; Gale, J. D.; Garcia, A.; Junquera, J.; Ordejon, P.; Sanchez-Portal, D. *J. Phys.: Condens. Matter* **2002**, *14*, 2745.
(39) Brandi, A.; Cardona, F.; Cicchi, S.; Cordero, F. M.; Goti, A. *Chem.—Eur. J.* **2009**, *15*, 7808.
(40) Goti, A.; Cicchi, S.; Cordero, F. M.; Fedi, V.; Brandi, A. *Molecules* **1999**, *4*, 1.
(41) Merino, P.; Tejero, T.; Revuelta, J.; Romero, P.; Cicchi, S.; Mannucci, V.; Brandi, A.; Goti, A. *Tetrahedron: Asymmetry* **2003**, *14*, 367.
(42) Revuelta, J.; Cicchi, S.; Goti, A.; Brandi, A. *Synthesis* **2007**, 485.
(43) Cardona, F.; Valenza, S.; Goti, A.; Brandi, A. *Tetrahedron Lett.* **1997**, *38*, 8097.
(44) Cardona, F.; Valenza, S.; Picasso, S.; Goti, A.; Brandi, A. *J. Org. Chem.* **1998**, *63*, 7311.
(45) Kocienski, P. J. *Protecting Groups*; 3rd ed.; Georg Thieme Stuttgart: New York, 2000.

(46) Cicchi, S.; Goti, A.; Brandi, A. *J. Org. Chem.* **1995**, *60*, 4743.

(47) Georgakilas, V.; Bourlinos, A.; Gournis, D.; Tsoufis, T.; Trapalis, C.; Mateo-Alonso, A.; Prato, M. *J. Am. Chem. Soc.* **2008**, *130*, 8733.

(48) Sing, K. S. W.; Everett, D. H.; Haul, R. A. W.; Moscou, L.; Pierotti, R. A.; Rouquérol, J. *Pure Appl. Chem.* **1985**, *57*, 603.

(49) Lee, Y. S.; Park, S.-H.; Lee, S. C.; Kim, H. J. *Chem. Phys. Lett.* **2006**, *432*, 518.

(50) Rather, S.; Zacharia, R.; Naik, M.; Hwang, S. W.; Kim, A. R.; Nahm, K. S. *Int. J. Hydrogen Energy* **2008**, *33*, 6710.

(51) Ströbel, R.; Garche, J.; Moseley, P. T.; Jörissen, L.; Wolf, G. *J. Power Source* **2006**, *159*, 781.

(52) Gregg, S. J.; Sing, K. S. W. *Adsorption, Surface Area and Porosity*, 2nd Ed.; Academic Press: London, 1982.

(53) Rouquérol, F.; Rouquérol, J.; Sing, K. S. W. *Adsorption by Powers and Porous Solids: Principles, Methodology and Applications*; Academic Press: London, 1999.

(54) Banks, C. E.; Compton, R. G. *Analyst* **2006**, *131*, 15.

(55) Banks, C. E.; Davies, T. J.; Wildgoose, G. G.; Compton, R. G. *Chem. Commun.* **2005**, 829.

(56) Leonhardt, A.; Ritschel, M.; Bartsch, K.; Graff, A.; Täschner, C.; Fink, J. *J. Phys. IV France* **2001**, *11*, Pr3.

(57) Thiên-Nga, L.; Bonard, J.-M.; Gáal, R.; Forro, L.; Hernadi, K. *Appl. Phys. Lett.* **2002**, *80*, 850.

(58) Wang, Y. Y.; Tang, G. Y.; Koeck, F. A. M.; Brown, B.; Garguilo, J. M.; Nemanich, R. J. *Diam. Relat. Mater.* **2004**, *13*, 1287.

(59) Wildgoose, G. G.; Banks, C. E.; Leventis, H. C.; Compton, R. G. *Microchim. Acta* **2006**, *152*, 187.

(60) Delhaes, P.; Couzi, M.; Trinquecoste, M.; Dentzer, J.; Hamidou, H.; Vix-Guterl, C. *Carbon* **2006**, *44*, 3005.

(61) Pumera, M. *Chem.—Eur. J.* **2009**, *15*, 4970.

(62) Amorin, R. G.; Fazzio, A.; Antonelli, A.; Novaes, F. D.; da Silva, A. J. R. *Nano Lett.* **2007**, *7*, 2459.

(63) Curran, S. A.; Talla, J. A.; Zhang, D.; Carroll, D. L. *J. Mater. Res.* **2005**, *20*, 3368.

(64) Telling, R. H.; Ewels, C. P.; El-Barbary, A. A.; Heggie, M. I. *Nat. Mater.* **2003**, *2*, 333.

(65) Kooi, S. E.; Schlecht, U.; Burghard, M.; Kern, K. *Angew. Chem., Int. Ed.* **2002**, *41*, 1353.

(66) Holloway, A. F.; Wildgoose, G. G.; Compton, R. G.; Shao, L.; Green, M. L. H. *J. Solid State Electrochem.* **2008**, *12*, 1337.

(67) Dresselhaus, M. S.; Dresselhaus, G.; Saito, R.; Jorio, A. *Phys. Rep.* **2005**, *409*, 47.

(68) Osswald, S.; Flahaut, E.; Ye, H.; Gogotsi, Y. *Chem. Phys. Lett.* **2005**, *402*, 422.

(69) Thomsen, C.; Reich, S. *Phys. Rev. Lett.* **2000**, *85*, 5214.

(70) Antunes, E. F.; Lobo, A. O.; Corat, E. J.; Trava-Airoldi, V. J.; Martin, A. A.; Verissimo, C. *Carbon* **2006**, *44*, 2202.

(71) Kurti, J.; Zolyomi, V.; Gruneis, A.; Kuzmany, H. *Phys. Rev. B* **2002**, *65*, 165433.

(72) Reich, S.; Thomsen, C. *Philos. Trans. R. Soc. London A* **2004**, *362*, 2271.

(73) Saito, R.; Gruneis, A.; Samsonidze, G. G.; Brar, V. W.; Dresselhaus, G.; Dresselhaus, M. S.; Jorio, A.; Cancado, L. G.; Fantini, C.; Pimenta, M. A.; Souza Filho, A. G. *New J. Phys.* **2003**, *5*, 157.1.

(74) Yang, D.-Q.; Rochette, J. F.; Sacher, E. *Langmuir* **2005**, *21*, 8539.

(75) Chakrapani, N.; Zhang, Y. M.; Nayak, S. K.; Moore, J. A.; Carroll, D. L.; Choi, Y. Y.; Ajayan, P. M. *J. Phys. Chem. B* **2003**, *107*, 9308.

(76) Jiang, C.; Kempa, K.; Zhao, J.; Schlecht, U.; Kolb, U.; Basché, T.; Burghard, M.; Mews, A. *Phys. Rev. B* **2002**, *66*, 161404.

(77) Bae, J. H.; Shanmugharaj, A. M.; Noh, W. H.; Choi, W. S.; Ryu, S. H. *Appl. Surf. Sci.* **2007**, *253*, 4150.

(78) Salavati-Niasari, M.; Bazarganipour, M. *Appl. Surf. Sci.* **2009**, *255*, 7610.

(79) Laine, R. N.; Vastola, F. J.; Walker, P. L. *J. Phys. Chem.* **1963**, *67*, 2030.

(80) Vix-Guterl, C.; Couzi, M.; Dentzer, J.; Trinquecoste, M.; Delhaes, P. *J. Phys. Chem. B* **2004**, *108*, 19361.

(81) Walker, P. L.; Taylor, R. L.; Ranish, J. M. *Carbon* **1991**, *29*, 411.

(82) Leon y Leon, C. A.; Radovic, L. R. *Chemistry and Physics of Carbon*; Marcel Dekker: New York, 1994; Vol. 24.

(83) Dresselhaus, M.; Dresselhaus, G.; Avouris, P. *Carbon Nanotubes: Synthesis, Properties and Applications*; Springer−Verlag: Berlin, 2001.

(84) Dresselhaus, M.; Dresselhaus, G.; Sugihara, K.; Spain, I. L.; Goldberg, H. A. *Graphite Fibers and Filaments*; Springer: Berlin, 1988.

(85) Bettinger, H. F. *Chem.—Eur. J.* **2006**, *12*, 4372.

(86) Saito, R.; Matsuo, R.; Kimura, T.; Dresselhaus, G.; Dresselhaus, M. S. *Chem. Phys. Lett.* **2001**, *348*, 187.

(87) Bettinger, H. F. *Org. Lett.* **2004**, *6*, 731.

(88) Mercuri, F.; Sgamellotti, A. *Phys. Chem. Chem. Phys.* **2009**, *11*, 563.

(89) Osuna, S.; Houk, K. N. *Chem.—Eur. J.* **2009**, *15*, 13219.

(90) Suenaga, K.; Wakabayashi, H.; Koshino, M.; Sato, Y.; Urita, K.; Iijima, S. *Nature Nanotechnol.* **2007**, *2*, 358.

(91) Valentini, L.; Mercuri, F.; Armentano, I.; Cantalini, C.; Picozzi, S.; Lozzi, L.; Santucci, S.; Sgamellotti, A.; Kenny, J. M. *Chem. Phys. Lett.* **2004**, *387*, 356.

(92) Mercuri, F.; Sgamellotti, A. *J. Phys. Chem. B* **2006**, *110*, 15291.

(93) Bettinger, H. F. *J. Phys. Chem. B* **2005**, *109*, 6922.

(94) Hashimoto, A.; Suenaga, K.; Gloter, A.; Urita, K.; Iijima, S. *Nature* **2004**, *430*, 870.

(95) Krasheninnikov, A. V.; Nordlund, K.; Sirvio, M.; Salonen, E.; Keinonen, J. *J. Phys. Rev. B* **2001**, *63*, 245405.

(96) Ma, Y. C.; Lehtinen, P. O.; Foster, A. S.; Nieminen, R. M. *New J. Phys.* **2004**, *6*, 68.

(97) Mercuri, F.; Sgamellotti, A.; Valentini, L.; Armentano, I.; Kenny, J. M. *J. Phys. Chem. B* **2005**, *109*, 13175.

(98) Mercuri, F.; Sgamellotti, A. *Inorg. Chim. Acta* **2007**, *360*, 785.

(99) Kotakoski, J.; Krasheninnikov, A. V.; Nordlund, K. *Phys. Rev. B* **2006**, *74*, 245420.

(100) Krasheninnikov, A. V.; Lehtiner, P. O.; Foster, A. S.; Nieminen, R. M. *Chem. Phys. Lett.* **2006**, *418*, 132.

(101) Lee, G. D.; Wang, C. Z.; Yoon, E.; Hwang, N. M.; Kim, D. Y.; Ho, K. M. *Phys. Rev. Lett.* **2005**, *95*, 205501.

(102) Tolvanen, A.; Kotakoski, J.; Krasheninnikov, A. V.; Nordlund, K. *Appl. Phys. Lett.* **2007**, *91*, 173109.

(103) Huhtala, M.; Krasheninnikov, A. V.; Aittoniemi, J.; Stuart, S. J.; Nordlund, K.; Kaski, K. *Phys. Rev. B* **2004**, *70*, 045404.

(104) Kanasaki, J.; Inami, E.; Tanimura, K.; Ohnishi, H.; Nasu, K. *Phys. Rev. Lett.* **2009**, *102*, 087402.

(105) Shan, B.; Cho, K. *Phys. Rev. B* **2006**, *73*, 081401.

(106) Lee, S. C.; Marzari, N. *Phys. Rev. Lett.* **2006**, *97*, 116801.

(107) Lee, Y. S.; Marzari, N. *J. Phys. Chem. C* **2008**, *112*, 4480.

(108) Baldoni, M.; Selli, D.; Sgamellotti, A.; Mercuri, F. *J. Phys. Chem. C* **2009**, *113*, 862.

(109) Chen, Z. F.; Nagase, S.; Hirsch, A.; Haddon, R. C.; Thiel, W.; Schleyer, P. V. *Angew. Chem., Int. Ed.* **2004**, *43*, 1552.

(110) Baldoni, M.; Sgamellotti, A.; Mercuri, F. *Chem. Phys. Lett.* **2008**, *464*, 202.

(111) Hu, L.; Hecht, D. S.; Grüner, G. *Chem. Rev.* **2010**, *110*, 5790.

(112) Andrews, R.; Weisenberger, M. C. *Curr. Opin. Solid State Mater. Sci.* **2004**, *8*, 31.

(113) McClory, C.; Chin, C. J.; McNally, T. *Aust. J. Chem.* **2009**, *62*, 762.

(114) Tjong, S. C. *Mater. Sci. Eng.* **2004**, *R 53*, 73.

(115) Hirsch, A. *Angew. Chem., Int. Ed.* **2002**, *41*, 1853.

(116) Li, J.; Qiu, J.-D.; Xu, J.-J.; Chen, H.-Y.; Xia, X.-H. *Adv. Funct. Mater.* **2007**, *17*, 1574.

(117) Lou, X.; Detrembleur, C.; Pagnoulle, C.; Jerome, R.; Bocharova, V.; Kiriy, A.; Stamm, M. *Adv. Mater.* **2004**, *16*, 2123.

(118) Mamedov, A. A.; Kotov, N. A.; Prato, M.; Guldi, D. M.; Wicksted, J. P.; Hirsch, A. *Nat. Mater.* **2002**, *1*, 190.

(119) Petrov, P.; Stassin, F.; Pagnoulle, C.; Jerome, R. *Chem. Commun.* **2003**, 2904.

(120) Sinani, V. A.; Gheith, M. K.; Yaroslavov, A. A.; Rakhnyanskaya, A. A.; Sun, K.; Mamedov, A. A.; Wicksted, J. P.; Kotov, N. A. *J. Am. Chem. Soc.* **2005**, *127*, 3463.

(121) Star, A.; Steuerman, D. W.; Heath, J. R.; Stoddart, J. F. *Angew. Chem., Int. Ed.* **2002**, *41*, 2508.

(122) Sui, X.-M.; Giordani, S.; Prato, M.; Wagner, H. D. *Appl. Phys. Lett.* **2009**, *95*, 233113.

(123) Jin, Z.; Sun, X.; Xu, G.; Goh, S. H.; Ji, W. *Chem. Phys. Lett.* **2000**, *318*, 505.

(124) Hong, S.; Kim, M.; Hong, C. K.; Jung, D.; Shim, S. E. *Synth. Met.* **2008**, *158*, 900.

(125) Zhao, X.; Lin, W.; Song, N.; Chen, X.; Fan, X.; Zhou, Q. *J. Mater. Chem.* **2006**, *16*, 4619.

(126) Pécastaings, G.; Delhaès, P.; Derré, A.; Saadaoui, H.; Carmona, F.; Cui, S. *J. Nanosci. Nanotechnol.* **2004**, *4*, 838.

(127) Herranz, M. A.; Ehli, C.; Campidelli, S.; Gutiérrez, M.; Hug, G. L.; Ohkubo, K.; Fukuzumi, S.; Prato, M.; Martin, N.; Guldi, D. M. *J. Am. Chem. Soc.* **2008**, *130*, 66.